coatings

MDPI

Article

Extracting the Optical Constants of Partially Absorbing TiO_2 ALD Films

Nimarta Kaur Chowdhary and Theodosia Gougousi *

Department of Physics, UMBC, Baltimore, MD 21250, USA
* Correspondence: gougousi@umbc.edu

Abstract: Typical titanium oxide (TiO_2) films are transparent in the visible range, allowing for their index of refraction and thickness to be extracted by single-angle spectroscopic ellipsometry (SE) using a Cauchy model. However, TiO_2 films grown by atomic layer deposition (ALD) from tetrakis(dimethylamino)titanium (IV) (TDMAT) and H_2O at 350°C are absorbing in the visible range due to the formation of Ti-O-N/Ti-N bonds. Single-angle SE is inadequate for extracting the optical constants of these films, as there are more unknowns (n, k, d) than measurable parameters (ψ, Δ). To overcome this limitation, we combined SE with transmission (T) measurements, a method known as SE + T. In the process, we developed an approach to prevent the backside deposition on quartz substrates during ALD deposition. When applying a B-spline model to SE + T data, film thicknesses on quartz substrates closely matched those on companion Si samples measured via standard lithography. The resulting optical constants indicate a reduced refractive index, n, and increased extinction coefficient, k, when compared to purer TiO_2 thin films deposited via a physical vapor deposition (PVD) method, reflecting the influence of nitrogen incorporation on the optical properties.

Keywords: Atomic Layer Deposition, Optical Characterization, Spectroscopic Ellipsometry

1. Introduction

Coatings with specific optical and electronic properties are critical for many technological applications including optoelectronics, photovoltaics, and sensors [1–4]. Atomic Layer Deposition (ALD) is a state-of-the-art technique that yields coatings with precise thickness control and a high degree of conformality. It is based on a self-limiting sequential chemistry in which the surface is exposed to the vapor of two or more reagents, designed to react in a complementary manner, and separated by purge steps to minimize gas-phase reactions [5]. This approach accomplishes good coverage, even in high-aspect-ratio structures and inside porous networks [6]. ALD coatings are widely used in applications such as anti-reflection and anti-glare coatings [7]. Therefore, the ability to characterize the optical properties of such coatings is fundamental to the advancement of the field.

Spectroscopic ellipsometry (SE) is a non-destructive, inexpensive, and efficient technique for characterizing thin films. It provides key properties such as thickness (d) and optical constants, including the index of refraction, n, and extinction coefficient (k), as a function of wavelength. The ellipsometric parameters, Psi (ψ) and Delta (Δ), are measured as functions of wavelength. They represent the change in polarization as light reflects from, or is transmitted through, a sample. The complex reflection ratio (Eqn. 1) is defined as the ratio of the reflectivity for p-polarized light (r_p) to the reflectivity for s-polarized light (r_s):

Citation: To be added by editorial staff during production.

Academic Editor: Firstname Lastname

Received: date
Revised: date
Accepted: date
Published: date

$$\tan(\psi)e^{i\Delta} = \rho = \frac{r_p}{r_s} \quad (1)$$

For transparent films, where k=0 in the visible range, film thickness and n can be extracted using an optical model, such as the Cauchy dispersion model [8,9]. However, for absorbing thin films, optical characterization is more complex due to a strong correlation between the optical constants and thickness [10]. Various approaches have been used for such cases, including determining the thickness in the region where k = 0, and then solving for n and d in the absorbing region [10]. Alternatively, optical parametrization techniques, such as B-spline [11], or general oscillator-based models (Lorentz, Gaussian, Tauc-Lorentz, Drude, Cody-Lorentz [10, 12, 13], etc.) may be used. Oscillator models are useful for identifying absorption transitions, but the parameters can become correlated as the number of oscillators increases, resulting in a loss of physical significance. B-spline models provide a more flexible and simpler alternative for absorbing materials with complex absorption [14] but lack the physical insight of oscillator models.

While these models can often provide plausible results, a high mean square error (MSE) and/or overfitting suggest that the solution may not be unique [15], especially when using ψ and Δ from a single angle measurement. Multiple-angle measurements can resolve this issue but may require appropriate substrate selection [10]. Alternatively, intensity-based transmission (T) measurements can supplement the single-angle data to achieve a fully determined solution.

In this manuscript, we apply the well-established SE + T technique [14, 15] to extract the optical functions of a series of absorbing TiO_2 films deposited by ALD. Transmission measurements at normal incidence (90°) supplement the ψ, Δ measurements taken at a fixed angle of 70°, giving three independent parameters (ψ, Δ, T) to solve for the three unknowns (n, k, d). This method requires a transparent substrate, like quartz, and care must be taken to prevent deposition on the sample's backside, which is challenging for a conformal deposition technique such as ALD. Backside deposition can interfere with the accuracy of SE + T measurements, leading to errors in the extracted optical functions. We present a sample mounting technique that minimizes the backside deposition on quartz substrates during the ALD process, ensuring accurate SE + T measurements and yielding physically meaningful optical functions. Reliable optical functions are critical for the design and optimal performance of optical devices, photovoltaics, sensors, and antireflection coating applications [1–4].

2. Experimental Methods:

2.1. Film Deposition

Absorbing TiO_2 films were grown using ALD, while control TiO_2 films were deposited by a Physical Vapor Deposition (PVD) method. Films were grown on double-polished P-type/Boron-doped Si (100), and quartz. The silicon substrates were cleaved from larger 4" wafers to assorted sizes and a mixture of quartz substrates cut from larger quartz sheets and pre-cut 1" by 1" pieces were used. The silicon-based substrates were cleaned sequentially in methanol (5 minutes) and acetone (5 minutes), and the quartz-based substrates were cleaned in acetone (10 minutes) and isopropanol (10 minutes). All substrates were rinsed in deionized (DI) water (5 minutes) and blown dry with N_2 gas before being loaded into the deposition chambers.

ALD TiO_2 thin films were deposited using a custom-built stainless steel hot wall flow tube reactor. The ALD chamber is described by Hackley [16] and is modeled after the reactor described in Ylilammi and Becker et al. [17, 18]. The ALD films were deposited at a substrate temperature of 350°C with a 5-second purge time with a varying number of cycles (thicknesses) using the tetrakis(dimethylamino)titanium (IV) (TDMAT) ($Ti[N(CH_3)_2]_4$, 99.999%, Sigma-Aldrich) precursor and deionized H_2O as the oxidizer. The TDMAT precursor was maintained at approximately 81°C, and H_2O was kept at room temperature. Both reagents were delivered to the system using the fixed-volume

approach described by Hausmann et al. [19]. During the ALD process, ultrahigh-purity N_2 was the buffer gas at an operating pressure between 260 – 290 mTorr. LabVIEW (National Instruments) was used to control the total number of cycles, dosage times, temperatures, and purge times. The sample pairs (quartz and silicon) were mounted side by side on the sample holder to ensure the samples were identical. Table I provides a summary of the films grown at 350°C.

Table I: Summary of ALD deposited samples. Samples marked 'A' are downstream and samples marked 'B' are upstream.

Sample Name	Number of Cycles	Temperature (°C)	Purge (s)
ALD 1	285	350	5
ALD 2A, B	350	350	5

Control TiO_2 films, referred to as "PVD TiO_2" in this work, were grown using non-reactive radio frequency (RF) magnetron sputtering in a Denton Vacuum DV-502A system with an Advanced Energy RFX 600 and ATX 600 RF Generator, using a TiO_2 target. Cleaned silicon and quartz substrates were mounted to a rotating chuck and kept at room temperature during depositions. The sputtering gas was 25 sccm of argon. Plasma was ignited at a power of 70W, and the power was slowly increased to its final RF power over 10 minutes. The target was cleaned with the shutter closed for 10 minutes before deposition. Films were not subject to any post-deposition treatment.

2.2. Sample Composition, Morphology and Transmission

X-ray photoelectron Spectroscopy (XPS) was used to study the composition of the resulting films. For this work, wide survey, and high-resolution elemental scans in the Ti 2p, N 1s, C 1s, and O 1s regions were conducted using a Kratos AXIS 165 spectrometer with an Al X-ray source (1486.6 eV) with a 0.1 eV step size. Some samples were scanned in the same regions using a Kratos AXIS ULTRA DLD XPS system equipped with an Al Kα X-ray source and a 165-mm mean radius electron energy hemispherical analyzer. Samples were analyzed as received. Spectra were fitted and the composition was extracted using CASA XPS. A JASCO V-570 UV/VIS/NIR Spectrophotometer measured the absorbance in the 200 nm – 2500 nm wavelength range.

Fourier transform infrared Spectroscopy (FTIR) was used to evaluate the film crystallinity and purity in the bulk using a Nicolet 4700 FTIR spectrometer in transmission mode. Spectra of 512 scans with a resolution of 4 cm^{-1} for the samples were collected using a deuterated triglycine sulfate detector (DTGS) and potassium bromide (KBr) beam splitter for the spectral range of 4000–400 cm^{-1} (mid-IR). A DTGS polyethylene (PE) detector with a solid substrate beam splitter was used for the spectral range of 600–50 cm^{-1} (far-IR). Data collection and analysis were conducted using the vendor-provided OMNIC software, and all spectra were ratioed to a native oxide silicon substrate.

2.3. Spectroscopic Ellipsometry

A J.A. Woollam alpha-SE Ellipsometer was used to measure ψ, Δ at 70° ('Off-Sample') and intensity-based transmission measurements at 90° ('Straight-Through') on quartz substrates. Transmission measurements were taken by adjusting the lever arms of the ellipsometer to the marked 90° position and placing the sample in the path of the beam. This combined method on transparent substrates is referred to as SE + T. Only ψ, Δ measurements at 70° were taken for the silicon substrates. All measurements were taken in the 380 – 900 nm (1.4 – 3.3 eV) wavelength range at the standard acquisition rate in three different spots.

For the most accurate SE measurements, the backside of the samples was covered with Scotch Magic Tape (cloudy finish), following the index-matching technique established in ref. [20]. This method suppresses backside reflections from the transparent substrate, as the refractive index of the Scotch tape is nearly equivalent to the refractive index of the quartz substrate; $n_{scotchtape} \approx n_{quartz} \approx 1.5$. The tape was removed using acetone and did not result in permanent damage to the film compared to other methods (i.e., roughening the backside). To minimize any errors related to tape contamination, the transmission measurements were taken before the SE measurements. To ensure the index-matching approach works effectively, the film deposition must be limited only to the top side of the quartz substrate, as any backside coatings will alter the reflections, influencing the SE data and results. The sample mounting approach that we have developed provides at least a region without such backside coatings during the ALD deposition process, making it compatible with the SE + T approach for optical characterization.

The combined SE and T measurements for each sample were then appended and simultaneously modeled [21]. For the ALD film, the 'Glass with Absorbing Film (with backside reflections)' model from the vendor-provided software was used. This model uses a '7059_Cauchy' substrate with a 1 mm thickness and a B-spline fitting layer [21]. The optical constants of this substrate layer sufficiently matched the optical constants of the substrates used in this work. Within the B-spline fitting layer, TiO_2 was used as the starting material ('Starting Mat'), and the resolution was set to 0.1 eV. Grading was applied within this layer. The 'Use KK mode' feature was enabled to ensure Kramers-Kronig consistency, while 'Surface roughness' and 'angle offset' were not used as fitting parameters. This approach provides the wavelength-dependent optical functions ($n(\lambda)$, $k(\lambda)$) and film thickness, d. For the transparent films, the 'Glass with Transparent Film' model from the vendor-provided software was used. This model uses a '7059_Cauchy' substrate with a Cauchy model. For the transparent films on silicon, a Cauchy model is used on the Si_jaw substrate with a 1.70 nm native oxide layer. The film thickness is confirmed by creating a step using standard lithography approaches on samples deposited on Si (100) and then using a KLA-Tencor Alpha Step 500 Profilometer for a step height measurement.

3. Results:

3.1. Producing ALD films with Single-Side Deposition

The approach we need to use for the extraction of the film's optical functions requires that deposition be limited to the sample's top side. One potential method to deal with backside coating was to use Kapton tape. However, adhesive residue is an issue. At temperatures above 300°C, tape burning and contamination of the films and deposition chamber are major concerns. Instead, a modified sample mounting approach was used, based on the idea of a 'sacrificial piece.'

More specifically, target quartz pieces were mounted on top of another quartz piece, or a polished silicon piece, and then the ALD process was executed. The idea behind this approach is that highly polished surfaces in contact limit the free space between the two stacked pieces substantially, which may suppress the conformal nature of the ALD process. Post-deposition, the presence of any backside deposition can be evaluated by performing appropriate measurements on the sacrificial pieces. If backside deposition has been suppressed, then the transmittance of a quartz sacrificial piece should be similar to that of a pristine quartz substrate. Similarly, for a Si sacrificial piece, SE measurements on the contact (top) surface should yield ψ and Δ values similar to those of pristine silicon.

Images and data regarding these samples are shown in Figure 1. Visual inspection (Fig.1a) indicates that there is little to no deposition on the quartz sacrificial piece, except along the edges. The average transmission values of the quartz sacrificial piece match the transmission values of a bare quartz substrate (Fig. 1b), suggesting no backside coating on the top quartz piece. In contrast, the Si sacrificial piece shows color variation, indicating the presence of a non-uniform coating. The average ψ and Δ values from the silicon

sacrificial piece (not shown) differ from those of pure silicon at all points on the surface, confirming deposition on the Si sacrificial piece and indicating deposition on the corresponding top quartz piece.

This is further supported by analyzing the respective quartz samples (Fig. 1a). The quartz sample mounted on the Si sacrificial piece appears darker, which indicates a larger optical thickness. Transmission measurements (not shown) confirm this observation: The 'quartz on silicon' sample exhibited decreased and non-uniform intensity, which may be due to a greater optical thickness. Based on these observations and measurements, we chose quartz substrates as sacrificial pieces.

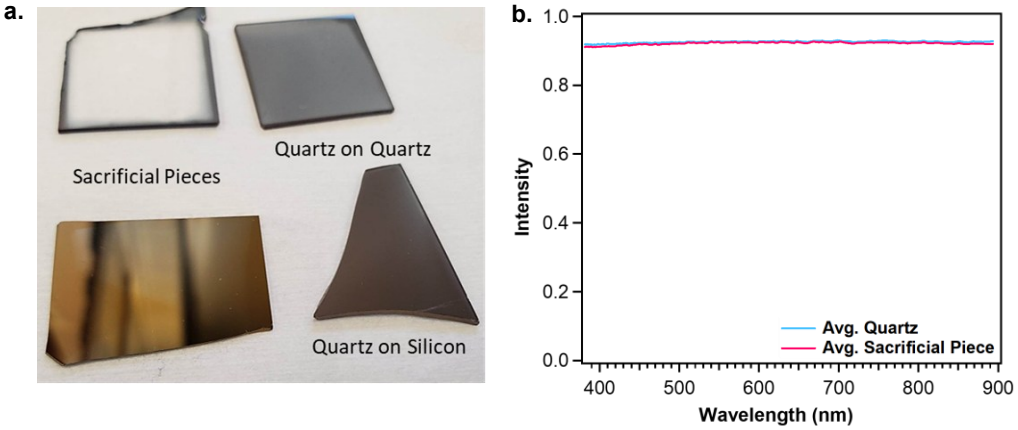

Figure 1: a.) Image of post-deposition samples and sacrificial pieces b.) Average transmission measurement through quartz sacrificial piece compared with average quartz substrate transmission intensity.

3.2. Composition and Morphology of the Films

The XPS survey scans for a PVD and an ALD sample (supporting information SI Fig. 1) confirm that the films are TiO_2 with varying concentrations of carbon and nitrogen-containing impurities. High-resolution spectra (Figure 2) for the Ti 2p region of the PVD TiO_2 film (Fig. 2a) show the Ti $2p_{3/2}$ peak at ~458.5 eV [22] and the Ti $2p_{1/2}$ peak at ~464.3 eV, associated with the Ti-O bond in TiO_2. ALD films grown at 350°C with a 5-second purge time are outside the optimal ALD growth window determined for this reactor. These parameters were chosen to further encourage precursor decomposition in a quasi-chemical vapor deposition (CVD) process [23]. With this temperature and purge time, XPS confirmed the presence of Ti-O-N/Ti-N metallic bonding within the films. Specifically, in the Ti 2p region, (Fig. 2a), a shoulder is observed in the binding energy range of ~455 – 457 eV [24] for the as-deposited ALD-grown films. This shoulder is absent in the PVD-grown films. Spectral deconvolution reveals two additional peaks – the feature at ~455 eV is associated with Ti-N bonding, while the peak at 457 eV is associated with TiO_xN_y [25]. Analysis of the N1s spectral region confirms this assignment.

In the N 1s region (Fig. 2b), the corresponding Ti-O-N and Ti-N peaks for the ALD film are observed at 396 and 397 eV, respectively [24], consistent with the peak assignment in the Ti 2p region. The other lower intensity peaks between 399 – 402 eV can be related to chemisorbed nitrogen [24,25] or amine-precursor ligands [26]. The N1s region for the PVD-grown film lacks any spectral features, in agreement with the Ti 2p region.

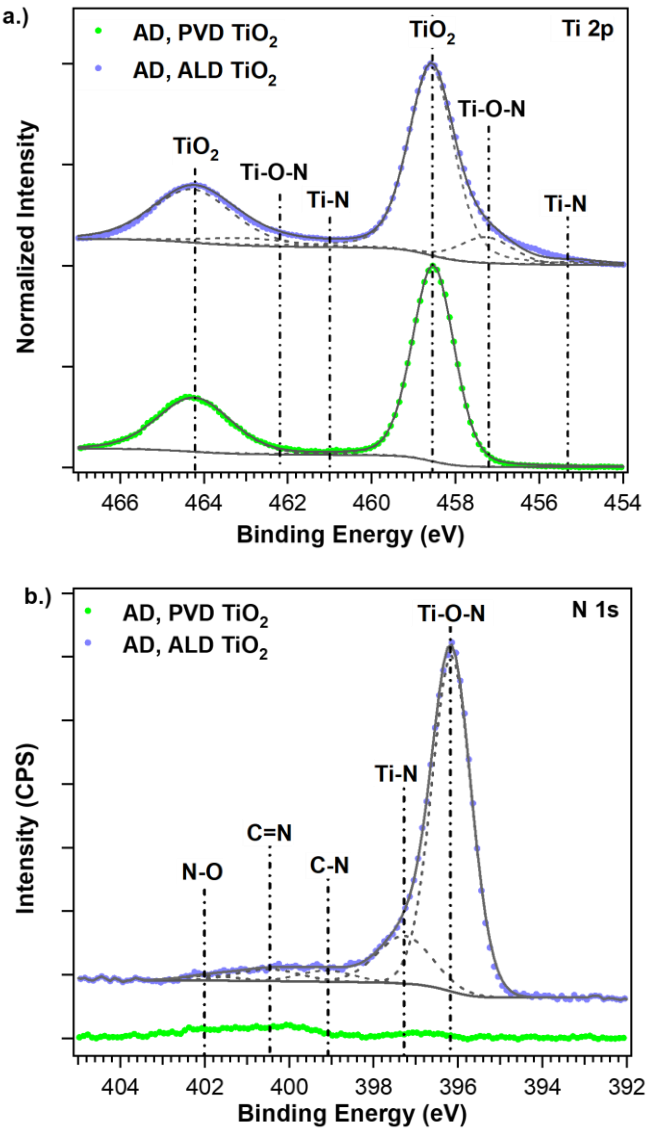

Figure 2: a. Ti 2p region b. N 1s region for as-deposited ALD (350°C) and PVD-grown TiO2 samples. Sample fits are included for the peaks in grey.

Composition analysis [27] indicates that the nitrogen (N) content in the films with this type of bonding is ~4.5 atomic percent (at.%) for the 350°C sample, higher than previously demonstrated [28], and 0% for the PVD TiO_2 film. The compositional analysis also shows that the 350°C film contains 22.8%, 45.9%, and 5.6% of Ti, O, and bonded C, respectively, while the PVD TiO_2 film contains 21.3%, 49.6%, and 2.8% of Ti, O, and bonded C, respectively. The PVD film contains less bonded carbon than the ALD film. This is illustrated by the C 1s region (SI Fig. 2), which reveals the presence of carbonate species for both films. Metal oxide films are susceptible to post-deposition reactions with atmospheric moisture and carbon dioxide, forming hydroxycarbonate species [29]. The mid-IR spectrum for the PVD film (SI Fig. 3) confirms the presence of carbonate species and adsorbed water from the ambient. Since XPS is a surface-sensitive technique, and reactions with atmospheric components are usually limited to the film surface, the measured carbon content for the PVD films should be regarded as an upper limit to the true value. Such small abundances of carbon are typical for all coatings, and the measured optical constants reflect that.

Additionally, high ALD deposition temperatures may result in partial or full film crystallization [30,31]. The far-IR region was used to assess crystallinity, revealing that all films analyzed in this work are mainly amorphous, as evidenced by broad peaks in the spectrum (SI Fig. 4). When the 350°C ALD film is annealed at 900°C for 10 minutes in an argon environment, distinct peaks are observed at 181 cm^{-1}, 375 cm^{-1} and 496 cm^{-1}, indicating the formation of the rutile phase of TiO_2 [32]. Previous work [33] has shown that FTIR data are consistent with X-ray diffraction (XRD) results when identifying phases in TiO_2 films, supporting FTIR's reliability for phase distinction in these samples. As a result, observed differences in optical functions can be primarily attributed to compositional differences rather than differences in crystallinity.

3.3. UV/VIS Absorption of the Films

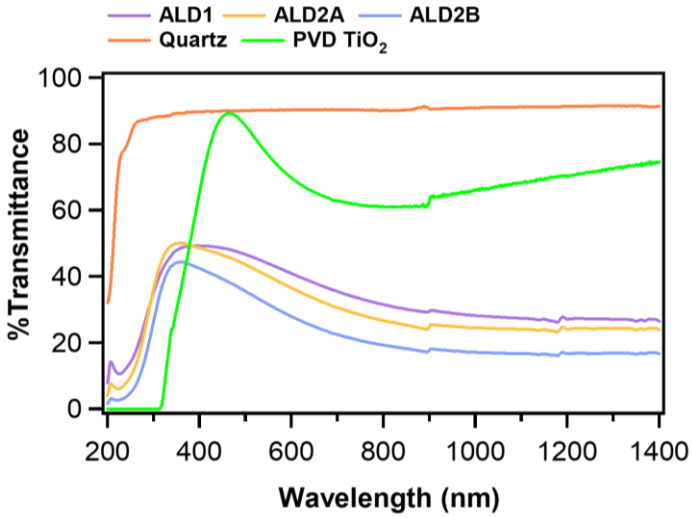

Figure 3: UV-Vis data for a series of TiO_2 films. The data for a quartz substrate is shown for reference.

Absorbance data from ultraviolet-visible (UV-VIS) spectroscopy was collected for the ALD and control PVD TiO_2 films. Transmittance was calculated from the raw absorbance data and the results are presented in Figure 3. Transmittance values of 100% indicate no absorption, while 0% indicates complete absorption. All ALD films deposited at 350°C show significant absorption in the visible range. In contrast, the PVD TiO_2 film exhibits high transmission, as expected [8, 34-36]. The high absorption of the ALD TiO_2 films can be traced to the presence of the oxynitride metallic bonding [37], confirmed by the XPS measurements. These results confirm that the ALD films are absorbing, necessitating additional information for extracting their optical functions.

3.4. Extracting the Optical Functions of the PVD TiO_2 Films

To ensure the validity of the SE + T method, the approach was initially tested on the transparent PVD TiO_2. A Cauchy model was used to model conventional ellipsometry measurements on Si (100) and for the SE + T approach on quartz. Both techniques returned similar values for the optical functions (Figure 4), with only slight differences at the lower wavelengths. Reported values for the refractive index (Fig. 4, green) can vary [38, 39] at the lower wavelengths due to differences in substrates and film growth [40]. The extinction coefficient (Fig. 4, orange) is zero for the visible wavelengths [41-43], but nonzero at ~400 nm, which is accurately described with both techniques.

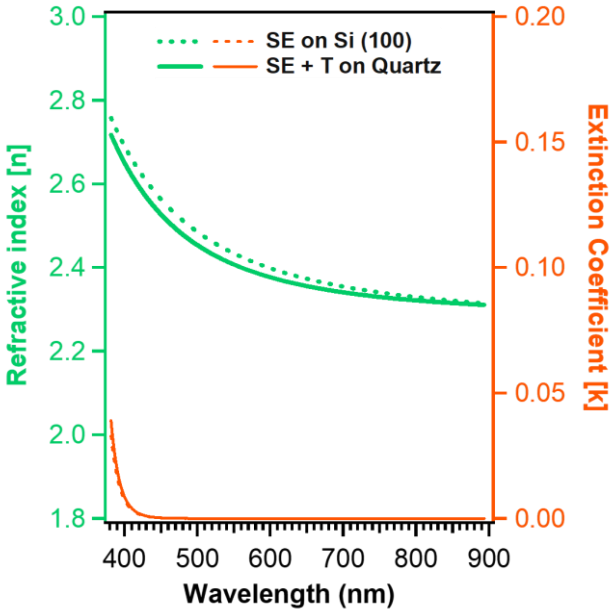

Figure 4: The optical functions for the PVD TiO_2 films on Si and Quartz.

The Cauchy fitting parameters (Table II) obtained for both methods are similar. The thickness results are consistent with the measured profilometer thickness. For thick samples, such as those in this work, MSE values around 10 are acceptable [21]. This benchmarks the SE + T method and ensures that SE + T can be used to determine accurate optical constants for the absorbing ALD TiO_2 films.

Table II: Summary of fit parameters for PVD TiO_2 films using the Cauchy model

Sample Substrate	A	B	C	Model Thickness	Surface Roughness	n @ 632.8 nm	MSE	Thickness (Profilometer)
Silicon	2.27	0.031	0.0058	91.1 ± 0.1 nm	2.6 ± 0.1 nm	2.38	7.9	96 ± 3.8 nm
Quartz	2.28	0.015	0.0071	92.7 ± 0.1 nm	4.0 ± 0.1 nm	2.36	8.3	

3.5. Extracting the Optical Functions of the ALD TiO_2 films

While the SE + T method is compatible with the ALD process and provides reasonable results for transparent films, it must be tested rigorously for absorbing films. This validation can be conducted by preparing samples with varied thicknesses (controlled by the number of ALD cycles) at 350°C with a 5-second purge and testing the sensitivity across three ALD samples. If there is no backside deposition and: i.) the SE + T measurements and modeling can simultaneously fit all ψ, Δ, and T measurements, ii.) accurately map thickness variations when compared to profilometry measurements, and iii.) yield a low MSE, then it is expected to provide reliable optical functions.

When operating outside the optimal ALD conditions, and especially at elevated temperatures, there may be significant precursor decomposition, resulting in thickness variations across the samples. To ensure consistency between the quartz and silicon measurements, we mounted quartz (on quartz SPs) and Si pieces side by side on the sample holder. Samples named "A" have been placed downstream of sample "B" on the sample holder for each deposition. For samples with no backside deposition, we evaluated the optical properties and thickness across three equivalent "spots" with multiple measurements for each spot. Sample fits of the SE and T experimental data are shown in Figure 5.

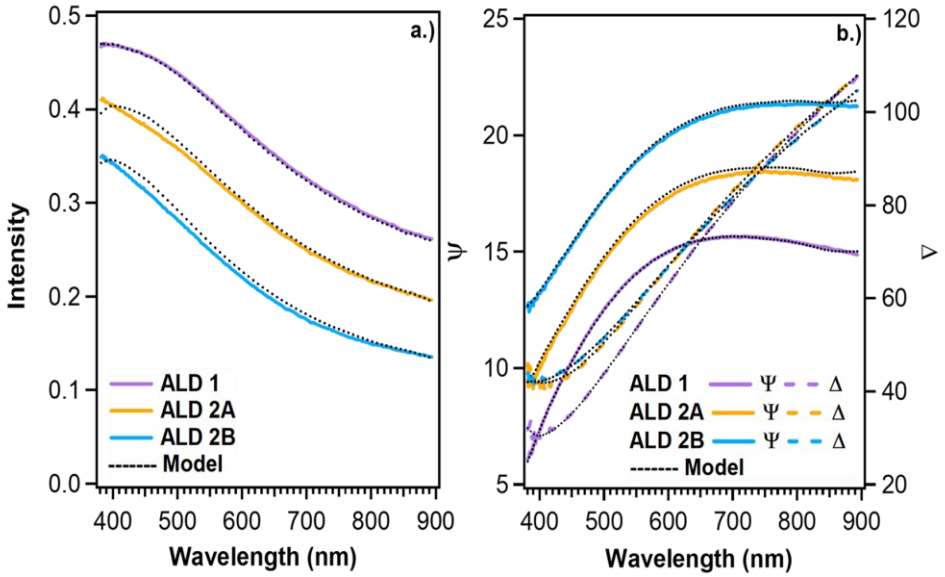

Figure 5: Simultaneously fitted a.) SE transmission (T) data b.) SE Psi/Delta (ψ, Δ) data for samples ALD 1 and ALD 2. The colored solid and dashed lines show measured experimental data, and the black dashed lines show the model fits.

The simple graded B-spline optical model can fit the experimental data accurately, as the model-generated data lie on top of the measured data set, reproducing all the structures and features simultaneously. The thickness obtained from the SE + T measurements and model on quartz can now be cross-checked with profilometer measurements on Si (100), as shown in Table III.

Table III: SE + T on Quartz and Profilometry on Si (100) Results for ALD TiO_2 film at 350°C.

Sample Name	SE + T Spot 1	Profilometer Spot 1	SE + T Spot 2	Profilometer Spot 2	SE + T Spot 3	Profilometer Spot 3
ALD 1	39.1 ± 0.3 nm	41.8 ± 0.8 nm	40.0 ± 0.1 nm	41.2 ± 1.4 nm	N/A	N/A
ALD 2A	49.9 ± 0.1 nm	49.6 ± 0.9 nm	49.1 ± 0.1 nm	49.0 ± 0.4 nm	48.2 ± 0.1 nm	50.1 ± 0.6 nm
ALD 2B	65.1 ± 0.1 nm	67.7 ± 1.3 nm	64.5 ± 0.1 nm	62.2 ± 1.0 nm	62.6 ± 0.1 nm	61.6 ± 0.8 nm

Considering the uncertainties, the SE + T thickness measurements on quartz and the profilometry thickness measurements on Si (100) are within approximately 5%. Additionally, we observe that films downstream (ALD 2A) are thinner than films upstream (ALD 2B), as shown by both profilometer measurements and optical modeling on SE + T data. This consistency supports the reliability of the SE + T method and the optical model used.

The optical functions between 380 – 900 nm for the three ALD samples are presented in Figure 6. The best fit for the data is obtained by assuming that the film is graded, with a non-constant index of refraction throughout the film bulk. Specifically, the film is divided into five sublayers, each with a linearly varying index of refraction. An average extinction coefficient is assumed for all layers, as varying it linearly does not improve the fit quality. Similar ALD films containing oxynitride bonds have been shown to exhibit a depth-varying composition due to ambient oxidation, validating the assumption of a varying index of refraction with film depth [28]. In contrast, grading the film did not change the optical functions of the as-deposited PVD TiO_2 films (Figure 6).

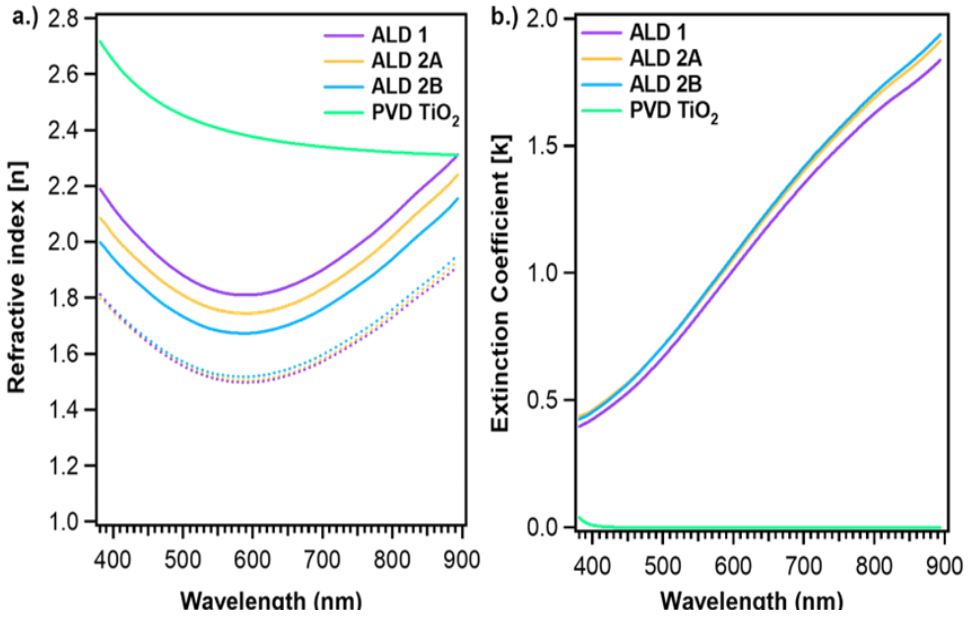

Figure 6: Optical functions a.) refractive index n, and b.) extinction coefficient k obtained using the SE + T approach with a graded B-spline model for the absorbing ALD TiO_2 films and a Cauchy model for the transparent PVD TiO_2 film. The top layer is represented by a solid line while the bottom layer is shown by a dashed line of the same color for each sample.

Comparing these results to the known physical characteristics of the samples can aid in evaluating the results. The ALD films contain TiO_2, TiO_xN_y, and TiN, as confirmed by XPS, and absorb in the visible range, as confirmed by UV-Vis. This suggests that their optical functions should differ from those of PVD TiO_2, which is indeed observed. The PVD TiO_2 films (Fig. 6a, green) have the highest n of the films in this work and k = 0 in the visible range (Fig. 6b, green), consistent with their measured high purity and their high transparency in the visible range.

For the ALD films, n decreases with wavelength until about 600 nm, then increases as a function of wavelength, while k only increases with wavelength. The measured refractive index n is somewhat higher and the extinction coefficient is somewhat lower than those reported for TiN films in the literature. Our films contain only about 4.5 at.% of Ti-N bonding; significantly less than the literature films. So overall, the optical functions are consistent with the composition of the films and the literature references [44]. Additionally, a lower n is measured for the bottom layers, which is compatible with a more TiN-like (greater oxynitride concentration) bottom layer, matching experimental observations [28].

These results capture the physical behavior of the ALD films, falling within the expected range between pure TiO_2 and pure TiN, as expected for this composition. Furthermore, the resulting MSE values are less than 3, which is reasonable for our experimental data. This further supports the reliability of the mounting approach, optical modeling, and resulting optical functions.

4. Conclusions

Single-angle spectroscopic ellipsometry is inadequate for extracting the optical functions of absorbing films because it provides an insufficient number of measurable parameters. Additionally, absorbing films deposited by ALD may also have backside deposition, which further complicates their optical characterization. To address these challenges, we used the SE+T technique in conjunction with a sample mounting approach that effectively eliminates backside deposition, allowing for the accurate determination of the film's optical functions and thickness. The method yields realistic optical functions and thickness values, which are validated by independent techniques.

Author Contributions: Conceptualization, Nimarta Chowdhary and Theodosia Gougousi; Formal analysis, Nimarta Chowdhary and Theodosia Gougousi; Funding acquisition, Theodosia Gougousi; Methodology, Nimarta Chowdhary and Theodosia Gougousi; Supervision, Theodosia Gougousi; Validation, Nimarta Chowdhary; Writing – original draft, Nimarta Chowdhary; Writing – review & editing, Theodosia Gougousi.

Data Availability Statement: The raw data supporting the conclusions of this article may be obtained from the authors upon reasonable request.

Acknowledgments: We thank Andrea Donohue from the Woollam facility for her time and help with the optical models. Also, thank you to Dr. Lisa Kelly and her graduate students from the Department of Chemistry and Biochemistry at UMBC for their help in obtaining UV-VIS data. Thank you to Dr. Ilkeun Lee at the University of California, Riverside, and Dr. Karen Gaskell at the University of Maryland, College Park for taking the XPS data. We would also like to thank Erik Crowe in the Physics Department at UMBC for machining the sample holder and transmission mounts. This material is based upon work supported by the National Science Foundation (NSF) under grant DMR-1905305.

Conflicts of Interest: The authors declare no conflicts of interest.

References

1. Yu, X.; Marks, T.J.; Facchetti, A. Metal Oxides for Optoelectronic Applications. *Nat. Mater.* **2016**, *15*, 383–396, doi:10.1038/nmat4599.

2. Choy, K.L. Chemical Vapour Deposition of Coatings. *Prog. Mater. Sci.* **2003**, *48*, 57–170, doi:10.1016/S0079-6425(01)00009-3.

3. Kaliyannan, G.V.; Palanisamy, S.V.; Priyanka, E.B.; Thangavel, S.; Sivaraj, S.; Rathanasamy, R. Investigation on Sol-Gel Based Coatings Application in Energy Sector – A Review. *Mater. Today Proc.* **2021**, *45*, 1138–1143, doi:10.1016/j.matpr.2020.03.484.

4. Mozumder, M.S.; Mourad, A.-H.I.; Pervez, H.; Surkatti, R. Recent Developments in Multifunctional Coatings for Solar Panel Applications: A Review. *Sol. Energy Mater. Sol. Cells* **2019**, *189*, 75–102, doi:10.1016/j.solmat.2018.09.015.

5. George, S.M. Atomic Layer Deposition: An Overview. *Chem. Rev.* **2010**, *110*, 111–131, doi:10.1021/cr900056b.

6. Detavernier, C.; Dendooven, J.; Sree, S.P.; F. Ludwig, K.; A. Martens, J. Tailoring Nanoporous Materials by Atomic Layer Deposition. *Chem. Soc. Rev.* **2011**, *40*, 5242–5253, doi:10.1039/C1CS15091J.

7. Ristok, S.; Flad, P.; Giessen, H. Atomic Layer Deposition of Conformal Anti-Reflective Coatings on Complex 3D Printed Micro-Optical Systems. *Opt. Mater. Express* **2022**, *12*, 2063, doi:10.1364/OME.454475.

8. Wang, X.; Wu, G.; Zhou, B.; Shen, J. Optical Constants of Crystallized TiO2 Coatings Prepared by Sol-Gel Process. *Materials* **2013**, *6*, 2819–2830, doi:10.3390/ma6072819.

9. Shamma, K.; Aldwayyan, A.; Albrithen, H.; Alodhayb, A. Exploiting the Properties of TiO_2 Thin Films as a Sensing Layer on (MEMS)-Based Sensors for Radiation Dosimetry Applications. *AIP Adv.* **2021**, *11*, 025209, doi:10.1063/5.0032353.

10. Hilfiker, J.N.; Singh, N.; Tiwald, T.; Convey, D.; Smith, S.M.; Baker, J.H.; Tompkins, H.G. Survey of Methods to Characterize Thin Absorbing Films with Spectroscopic Ellipsometry. *Thin Solid Films* **2008**, *516*, 7979–7989, doi:10.1016/j.tsf.2008.04.060.

11. Rafieian, D.; Ogieglo, W.; Savenije, T.; Lammertink, R.G.H. Controlled Formation of Anatase and Rutile TiO_2 Thin Films by Reactive Magnetron Sputtering. *AIP Adv.* **2015**, *5*, 097168, doi:10.1063/1.4931925.

12. Zeiss, C. Application of the Tauc-Lorentz Formulation to the Interband Absorption of Optical Coating Materials. **2001**.

13. Wang, L.; Liu, H.; Li, S.; Jiang, C.; Ji, Y.; Chen, D. Study on the Composite Dispersion Model of Optical Constants of Metal-Oxide Films in the Range from Ultraviolet to near Infrared. *Optik* **2018**, *168*, 892–900, doi:10.1016/j.ijleo.2018.05.019.

14. Hilfiker, J.N.; Linford, M.R. Fitting the Spectroscopic Ellipsometry Data from a Rather Thick (Organic?) Film on Fused Silica. *Vac. Technol. Coat.* **2022**.

15. Hilfiker, J.N.; Linford, M.R. Combining Spectroscopic Ellipsometry and Transmission Spectrophotometric Data for the Analysis of Thin Metal Films. *Vac. Technol. Coat.* **2022**.
16. Hackley, J.C.; Gougousi, T.; Demaree, J.D. Nucleation of HfO2 Atomic Layer Deposition Films on Chemical Oxide and H-Terminated Si. *J. Appl. Phys.* **2007**, *102*, 034101, doi:10.1063/1.2764223.
17. Ylilammi, M. Monolayer Thickness in Atomic Layer Deposition. *Thin Solid Films* **1996**, *279*, 124–130, doi:10.1016/0040-6090(95)08159-3.
18. Becker, J.S.; Kim, E.; Gordon, R.G. Atomic Layer Deposition of Insulating Hafnium and Zirconium Nitrides. *Chem. Mater.* **2004**, *16*, 3497–3501, doi:10.1021/cm049516y.
19. Hausmann, D.M.; de Rouffignac, P.; Smith, A.; Gordon, R.; Monsma, D. Highly Conformal Atomic Layer Deposition of Tantalum Oxide Using Alkylamide Precursors. *Thin Solid Films* **2003**, *443*, 1–4, doi:10.1016/S0040-6090(03)00502-9.
20. Synowicki, R.A. Suppression of Backside Reflections from Transparent Substrates. *Phys. Status Solidi C* **2008**, *5*, 1085–1088, doi:10.1002/pssc.200777873.
21. J. A. Woollam Co., Inc. CompleteEASE Data Analysis Manual 2011.
22. Stefanov, P.; Shipochka, M.; Stefchev, P.; Raicheva, Z.; Lazarova, V.; Spassov, L. XPS Characterization of TiO_2 Layers Deposited on Quartz Plates. *J. Phys. Conf. Ser.* **2008**, *100*, 012039, doi:10.1088/1742-6596/100/1/012039.
23. Driessen, J.P.A.M.; Schoonman, J.; Jensen, K.F. Infrared Spectroscopic Study of Decomposition of $Ti(N(CH_3)_2)_4$. *J. Electrochem. Soc.* **2001**, *148*, G178–G184, doi:10.1149/1.1350687.
24. Song, X.; Gopireddy, D.; Takoudis, C.G. Characterization of Titanium Oxynitride Films Deposited by Low Pressure Chemical Vapor Deposition Using Amide Ti Precursor. *Thin Solid Films* **2008**, *516*, 6330–6335, doi:10.1016/j.tsf.2007.12.148.
25. Khwansungnoen, P.; Chaiyakun, S.; Rattana, T. Room Temperature Sputtered Titanium Oxynitride Thin Films: The Influence of Oxygen Addition. *Thin Solid Films* **2020**, *711*, 138269, doi:10.1016/j.tsf.2020.138269.
26. Olayo, M.G.; Alvarado, E.J.; González-Torres, M.; Gómez, L.M.; Cruz, G.J. Quantifying Amines in Polymers by XPS. *Polym. Bull.* **2024**, *81*, 2319–2328, doi:10.1007/s00289-023-04829-y.
27. Shard, A.G. Practical Guides for X-Ray Photoelectron Spectroscopy: Quantitative XPS. *J. Vac. Sci. Technol. A* **2020**, *38*, 041201, doi:10.1116/1.5141395.
28. Kuis, R.; Gougousi, T.; Basaldua, I.; Burkins, P.; Kropp, J.A.; Johnson, A.M. Engineering of Large Third-Order Nonlinearities in Atomic Layer Deposition Grown Nitrogen-Enriched TiO_2. *ACS Photonics* **2019**, *6*, 2966–2973, doi:10.1021/acsphotonics.9b01176.
29. Gougousi, T.; Parsons, G. Postdeposition Reactivity of Sputter-Deposited High-Dielectric-Constant Films with Ambient H2O and Carbon-Containing Species. *J. Appl. Phys.* **2004**, *95*, 1391–1396, doi:10.1063/1.1636513.

30. Aarik, J.; Aidla, A.; Uustare, T.; Sammelselg, V. Morphology and Structure of TiO2 Thin Films Grown by Atomic Layer Deposition. *J. Cryst. Growth* **1995**, *148*, 268–275, doi:10.1016/0022-0248(94)00874-4
31. Kim, S.K.; Hoffmann-Eifert, S.; Reiners, M.; Waser, R. Relation Between Enhancement in Growth and Thickness-Dependent Crystallization in ALD TiO2 Thin Films. *J. Electrochem. Soc.* **2010**, *158*, D6, doi:10.1149/1.3507258
32. Schöche, S.; Hofmann, T.; Korlacki, R.; Tiwald, T.E.; Schubert, M. Infrared Dielectric Anisotropy and Phonon Modes of Rutile TiO_2. *J. Appl. Phys.* **2013**, *113*, 164102, doi:10.1063/1.4802715
33. Henegar, A.J.; Gougousi, T. Stability and Surface Reactivity of Anatase TiO_2 Films. *ECS J. Solid State Sci. Technol.* **2015**, *4*, P298–P304, doi:10.1149/2.0041508jss
34. Abdel-Aziz, M.M.; Yahia, I.S.; Wahab, L.A.; Fadel, M.; Afifi, M.A. Determination and Analysis of Dispersive Optical Constant of TiO2 and Ti2O3 Thin Films. *Appl. Surf. Sci.* **2006**, *252*, 8163–8170, doi:10.1016/j.apsusc.2005.10.040.

35. Ghrairi, N.; Bouaicha, M. Structural, Morphological, and Optical Properties of TiO2 Thin Films Synthesized by the Electro Phoretic Deposition Technique. *Nanoscale Res. Lett.* **2012**, *7*, 357, doi:10.1186/1556-276X-7-357.

36. Sreemany, M.; Sen, S. A Simple Spectrophotometric Method for Determination of the Optical Constants and Band Gap Energy of Multiple Layer TiO2 Thin Films. *Mater. Chem. Phys.* **2004**, *83*, 169–177, doi:10.1016/j.matchemphys.2003.09.030.

37. Demeter, A.; Samoila, F.; Tiron, V.; Stanescu, D.; Magnan, H.; Straticiuc, M.; Burducea, I.; Sirghi, L. Visible-Light Photocatalytic Activity of TiO x N y Thin Films Obtained by Reactive Multi-Pulse High Power Impulse Magnetron Sputtering. *Surf. Coat. Technol.* **2017**, *324*, 614–619, doi:10.1016/j.surfcoat.2016.10.011.

38. Refractive Index and Degree of Inhomogeneity of Nanocrystalline TiO2 Thin Films: Effects of Substrate and Annealing Temperature. *J Appl Phys* **2000**, *88*, 9.

39. Kasikov, A.; Aarik, J.; Mändar, H.; Moppel, M.; Pärs, M.; Uustare, T. Refractive Index Gradients in TiO_2 Thin Films Grown by Atomic Layer Deposition. *J. Phys. Appl. Phys.* **2006**, *39*, 54–60, doi:10.1088/0022-3727/39/1/010.

40. Jolivet, A.; Labbé, C.; Frilay, C.; Debieu, O.; Marie, P.; Horcholle, B.; Lemarié, F.; Portier, X.; Grygiel, C.; Duprey, S.; et al. Structural, Optical, and Electrical Properties of TiO2 Thin Films Deposited by ALD: Impact of the Substrate, the Deposited Thickness and the Deposition Temperature. *Appl. Surf. Sci.* **2023**, *608*, 155214, doi:10.1016/j.apsusc.2022.155214.

41. Saha, D.; Ajimsha, R.S.; Rajiv, K.; Mukherjee, C.; Gupta, M.; Misra, P.; Kukreja, L.M. Spectroscopic Ellipsometry Characterization of Amorphous and Crystalline TiO 2 Thin Films Grown by Atomic Layer Deposition at Different Temperatures. *Appl. Surf. Sci.* **2014**, *315*, 116–123, doi:10.1016/j.apsusc.2014.07.098.

42. Kim, S.Y. Simultaneous Determination of Refractive Index, Extinction Coefficient, and Void Distribution of Titanium Dioxide Thin Film by Optical Methods. *Appl. Opt.* **1996**, *35*, 6703–6707, doi:10.1364/AO.35.006703.

43. Mardare, D.; Stancu, A. On the Optical Constants of TiO2 Thin Films. Ellipsometric Studies. *Mater. Res. Bull.* **2000**, *35*, 2017–2025, doi:10.1016/S0025-5408(00)00408-6.

44. Ali, S.; Magnusson, R.; Pshyk, O.; Birch, J.; Eklund, P.; Le Febvrier, A. Effect of O/N Content on the Phase, Morphology, and Optical Properties of Titanium Oxynitride Thin Films. *J. Mater. Sci.* **2023**, *58*, 10975–10985, doi:10.1007/s10853-023-08717-8.